Electronic Supplementary Material (ESI) for Materials Horizons.

Electronic Supplementary Information for

Factors Affecting Bismuth Vanadate Photoelectrochemical Performance

Timothy S. Sinclair, Bryan M. Hunter, Jay R. Winkler, Harry B. Gray, Astrid M. Müller*

Beckman Institute and Division of Chemistry and Chemical Engineering, California Institute of Technology, Pasadena, California 91125; correspondence should be addressed to astridm@caltech.edu.

1. Reported $BiVO_4$ photoanode performances

Table S1. Reported photocurrent densities j_{ph} (at 1.23 V vs. RHE, with 1 sun AM1.5G front-side illumination) of undoped, bare $BiVO_4$ without sub-layers or co-catalysts on transparent conducting oxide substrates. KP_i, potassium phosphate buffer; KB_i, potassium borate buffer. It should be noted that, for comparability reasons, only reports with photocurrent measurements at 1 sun, AM1.5G illumination were considered.

Reference	$BiVO_4$ film preparation method	j_{ph} (mA cm^{-2})	Aqueous Electrolyte	j_{ph} (mA cm^{-2}) with hole acceptor	Aqueous electrolyte with hole acceptor	Scan rate (mV s^{-1})	Transparent conducting oxide substrate
1	Chemical bath deposition	<0.05	0.5 M Na_2SO_4	–	–	50	FTO, TEC-15
2	Spin-coating	0.2	1.0 M Na_2SO_4	–	–	10	FTO, 10 Ω/sq., Nippon Sheet Glass Co.
3	Reactive ballistic deposition	0.2	1.0 M KP_i + 0.5 M Na_2SO_4, pH 7.0	0.4	1.0 M KP_i + 0.5 M Na_2SO_4, pH 7.0 + 0.5 M Na_2SO_3	25	FTO, Pilkington TEC-15
4	Electrodeposition	0.1	0.1 M KP_i, pH 7.0	1.9	0.1 M KP_i, pH 7.0 + 0.1 M Na_2SO_3	10	FTO, Hartford Glass Inc.
5	Spray pyrolysis	0.7	0.5 M K_2SO_4 + KP_i pH 5.6 or 0.1 M KP_i, pH 7.0	1.8	0.5 M K_2SO_4 + KP_i pH 5.6 or 0.1 M KP_i, pH 7.0 + 0.5 M H_2O_2	50	FTO, Hartford Glass Inc., TEC-15
6	Spin-coating	0.25	0.1 M KP_i, pH 7.0	0.7	0.1 M KP_i, pH 7.0 + 0.05 M H_2O_2	10	FTO, Pilkington
7	Spin-coating	0.3	0.1 M KB_i, pH 9.2	–	–	10	FTO, Pilkington
8	Reactive sputtering	0.44	0.1 M KP_i + 0.5 M Na_2SO_4, pH 7.0	–	–	Not reported	ITO, source not specified
9	Chemical vapour deposition	–	–	0.28	0.1 M K_2HPO_4 buffer, pH 7.0 + 0.5 M Na_2SO_3	Not reported	FTO, source not specified
10	Electrodeposition + chemical conversion	1.8	0.1 M KP_i, pH 7.0	4.7	0.1 M KP_i, pH 7.0 + 1 M Na_2SO_3	10	FTO, source not specified

2. Experimental details

Materials and Methods

XPS, optical spectroscopy, and PEC experiments were performed at the Molecular Materials Research Center (Beckman Institute at California Institute of Technology). SEM images were collected at the California Institute of Technology GPS Division Analytical Facility.
All chemicals were purchased in the indicated grade and used as received. All water used in this work was of high purity and obtained from a Barnstead Diamond Nanopure system with a resistivity of ≥ 16 MΩ cm.
Data analysis, unless otherwise noted, and graphing were performed with Igor Pro 6.34 (WaveMetrics, Inc.); 3D bar graphs were generated with Matlab R2013b (MathWorks, Inc.).

Photoanode Preparation

All $BiVO_4$ films were prepared on FTO-glass substrates purchased from Hartford Glass Co. (surface resistivity ~13 Ω/sq, TEC 15). All FTO-glass pieces, except those for electrodeposition without added iodide, were cleaned as follows: they were (i) rinsed with water and patted dry with a Kimwipe, (ii) rinsed with acetone (EMD, HPLC grade) and patted dry with a Kimwipe, (iii) surface-etched by submerging for 5 seconds in concentrated hydrochloric acid (Macron), rinsed with water, and patted dry with a Kimwipe. The FTO-substrates were used immediately after cleaning. FTO-glass for electrodeposition without added iodide was etched for 20 minutes in Piranha solution, which was composed of a 3:1 (v:v) mixture of concentrated sul-

phuric acid (J.T.Baker) and 30% aqueous hydrogen peroxide solution (EMD), rinsed with water, and dried in a nitrogen stream.

For electrodeposition baths, 0.035 M vanadium(IV) sulfate oxide hydrate (Alfa, 99.9%) and 0.010 M bismuth(III) nitrate pentahydrate (Sigma-Aldrich, ≥98%) were added to 50 mL 1.0 M aqueous nitric acid (EMD), in accordance with Choi's report.[4] In case of added iodide in the plating bath, 0.04 M, 0.08 M, or 0.12 M sodium iodide (Mallinckrodt, analytical reagent grade) were added to 50 mL of this stock solution, to reach $[I^-]/[Bi^{3+}]$ ratios of 4, 8, or 12, respectively.

Electrodeposited $BiVO_4$ films were prepared from these plating solutions in a 7-cm diameter crystallization dish, which was held at (70 ± 0.5) °C. A freshly cleaned FTO-glass piece (~3 cm × 5 cm) was placed vertically and about two thirds submerged in the plating bath. The deposition solution was stirred rapidly, without the stir bar touching the FTO-glass piece.

The FTO-glass piece (working electrode) was connected to an alligator clip, which was kept dry; a Ni gauze (Alfa) counter electrode and an Ag/AgCl/3.0 M NaCl reference electrode (Bioanalytical Systems, Inc.) were used. Just prior to applying a potential, 1.7 M sodium acetate trihydrate (Mallinckrodt, 99.9%) was added to the solution to adjust the pH to 4.7. Using a Princeton Applied Research Parstat 4000 potentiostat, Bi–V–O films were potentiostatically deposited on FTO; a potential of 1.9 V vs. Ag/AgCl was applied for 300 seconds, passing 5 C of charge. All electrodeposited films were rinsed with water and dried in ambient air.

Monoclinic scheelite $BiVO_4$ films on FTO-glass were obtained by annealing in ambient air for 6 hours at 500 °C, with a ramping rate of 2 °C per minute. This way, the amorphous deposit was converted into crystalline $BiVO_4$ and amorphous V_2O_5, in accordance with Choi's report.[4] Vanadium oxide was dissolved in 0.1 M pH 13.0 aqueous KOH (J.T.Baker, N.F.) for 20 minutes, after which the films were rinsed with water and dried in ambient air.

Spin coated $BiVO_4$ films were prepared on ~ 3 cm × 10 cm FTO-glass substrates, with an area of the FTO slide masked with Scotch tape to provide bare FTO for electrical contact. Two different precursor solutions were used. One was a solution of 0.06 M vanadyl bis(acetylacetonate) (Sigma-Aldrich, 99.99%) and 0.06 M bismuth(III) nitrate pentahydrate (Sigma-Aldrich, ≥98%) in a 1:9 (v:v) mixture of glacial acetic acid (J.T.Baker, 99.9%) and 2,4-pentanedione (Sigma-Aldrich, ≥98%), in accordance with Gamelin's report.[11] The other was a modification of this published procedure and had a higher viscosity. In this case, the solvent was a 1:8:1 mixture of glacial acetic acid, 2,4-pentanedione, and polyethylene glycol (PEG; Sigma Life Sciences, BioUltra 400).

Slides were spin coated for 2, 4, 6, or 8 cycles. A spin-coating cycle consisted of two times pipetting 320 µL of precursor solution drop by drop onto an FTO slide spinning at 1,000 rpm for 30 seconds, and then placing the slide in a kiln at 500 °C for 10 minutes in ambient air. After the last overall cycle, the slides were annealed at 500 °C for 2 hours in ambient air.

FTO slides with electrodeposited and spin-cast $BiVO_4$ films were subdivided by scribing and breaking them into ~ 1.0 cm × 2.5 cm pieces. All electrodes had some bare FTO, to which a silver-coated copper wire was firmly attached with silver paint (SPI, high purity). For mechanical stability the wire was run inside a glass tube, whose end and all exposed conducting parts were sealed with an epoxy adhesive (Loctite Hysol 9460). To obtain the same defined area of exposed $BiVO_4$ (0.079 cm^2) on each electrode, part of the $BiVO_4$ film was masked with a 3.2-mm diameter metal disk and spray-painted with black high-temperature paint (McMaster-Carr). We tested the chemical stability of this paint in our electrolytes and confirmed that it was stable for hours, which was much longer than the measurement time.

Physical Characterization

Film thicknesses were determined via optical spectroscopy. UV/vis data were measured with a Cary 5000 dual beam spectrophotometer, which was equipped with an integrating sphere and a centre mount sample

holder. This permitted the collection of transmission spectra without interference from normally reflected light from the scattering surface of the solid films. Absorptances *Abs* were calculated from measured baseline-corrected transmissions *T*, using the equation $Abs = -\ln(T)$. The absorptance spectrum of bare FTO-glass was subtracted from all absorptance spectra of $BiVO_4$ films on FTO-glass. $BiVO_4$ film thicknesses were derived using absorption coefficients reported for powder $BiVO_4$.[12]

Crystal phases were identified from powder x-ray diffraction (XRD) data. The usual information depth of XRD measurements ranges from a few micrometres to a few hundred micrometres, depending on the density of the material. Therefore, this method probes the entire $BiVO_4$ films. In contrast, information on chemical surface compositions was obtained by x-ray photoelectron spectroscopy (XPS). Typical escape depths of photoelectrons are on the order of a few nanometres, thereby limiting the probe depths of XPS experiments to materials surfaces. Surface compositions of photoanodes matter because they affect how efficiently charge carriers are transported across interfaces, such as into a catalyst or electrode material, and surface defects are a major source for carrier recombination losses. Surface morphologies, obtained from scanning electron microscopy (SEM) images, provided insights into the microscopic surface structures. We quantified morphology by analysing distributions of crystallite areas and diameters that were normalised to the crystallites' aspect ratios. A Bruker D2 PHASER diffractometer with monochromatic Cu Kα radiation (1.5418 Å; tube power 30 kV, 10 mA) was used; it was equipped with 0.1° divergence, 1.5° Soller, and 0.6 mm detector slits, and had a 3-mm secondary anti-scatter screen. Diffracted radiation was collected with a Lynxeye detector. The resolution was 0.05° in 2θ, and the counting time was 3 s per step, resulting in a total scan time of about 75 min for each sample. The as-prepared $BiVO_4$ films on FTO-glass were placed at the correct height in the instrument with a custom-built acrylic sample holder. XRD pattern analysis was performed with the Bruker DIFFRAC.SUITE software coupled to the International Centre for Diffraction Data powder diffraction file database (ICDD, PDF-2 Release 2012).

XPS data were collected using a Surface Science Instruments M-probe surface spectrometer. Monochromatic Al Kα radiation (1486.6 eV) was used to excite electrons of the $BiVO_4$ films on FTO-glass. The sample chamber was maintained at $<7\times10^{-9}$ mbar. Survey scans from 0 to 1100 eV were carried out to identify the elements present. Binding energies were referenced to the C 1s peak arising from adventitious carbon, taken to have a binding energy of 284.8 eV.[13] High-resolution spectra were collected for the Bi 4d, V 2p and O 1s core level regions; in case of materials that were made with NaI in the electrodeposition bath, additionally high-resolution spectra were collected in the I 3d region. Integration of Bi $4d_{5/2}$ and V $2p_{3/2}$ peak intensities after Shirley background subtraction,[14] weighted by relative atomic sensitivity factors, yielded a quantification of surface Bi/V ratios. Quantitative XPS analysis was performed with CasaXPS (Version 2.3.16 PR 1.6).

Resistivity measurements were performed using a Jandel four-point test station with a tungsten carbide probe. All current-voltage responses were ohmic. For all measurements the same correction factor of 4.54 was applied. Thicknesses obtained from optical spectroscopy were used.

Morphologies were obtained from SEM images. They were collected with a Zeiss LEO 1550VP Field-Emission SEM, operated at 5 kV and a working distance of 11 mm, with the sample stage tilted at 0° (top-down view) or 90° (cross-sectional view). As-prepared $BiVO_4$ on FTO-glass samples were fixed to the sample stage with carbon tape, which was wrapped around to the top of each sample to electrically ground the $BiVO_4$ films to the stage and minimise charging effects. Cross-sectional samples were coated with 11 nm Au/Pd (80/20, density 17.84 g cm^{-2}, Ted Pella), to minimise space charge distortions of the image from the non-conducting glass substrate. A Cressington sputter coater (model 208 HR) with a Cressington thickness controller (model mtm 20) was used, the pressure was kept below 1×10^{-3} mbar, and the current was 80 mA.

Morphologies were quantified by two different techniques. We derived crystallite areas as SEM images are most commonly analysed this way. We also deduced crystallite diameters that were normalised to their aspect ratios. For both methods, collected micrographs were transformed into threshold images, and ellipses

were fitted to crystallite edges, using the ImageJ software.[15] From these ellipse fits, we derived histograms for the crystallite areas *a* and the aspect-ratio-normalised diameters *l*, defined as an ellipse's semi-minor axis divided by its semi-major axis times the square root of its area. The first (mean), second (variance), third (skew), and fourth (kurtosis) moments of both types of distributions were determined numerically, using Matlab R2013b (MathWorks, Inc.). The grouped data were given values of the ellipse fits bin midpoint. The mean was calculated about the origin, while the n^{th} moments ($n > 1$) were calculated about the mean as:

$$m_n = \frac{\sum(x_i - \bar{x})^n}{N}$$

where *N* was the total number of observed crystallites. The mean values of *a* and *l* are denoted *A* and *L*, respectively.

Photoelectrochemistry

Linear sweep and cyclic voltammograms of $BiVO_4$ on FTO-glass electrodes were collected with a Princeton Applied Research model 362 potentiostat at room temperature and in ambient air (scan rate 10 mV s^{-1}). Forward and reverse sweeps showed minimal hysteresis. Electrochemical experiments were carried out in a standard Pyrex three-electrode single-compartment electrochemical cell equipped with a flat quartz window for illumination. All potentials reported here are relative to the reversible hydrogen electrode (RHE). PEC performance was assessed in 0.1 M (pH 13.0) aqueous KOH or 0.1 M (pH 13.0) aqueous KOH with 0.5 M Na_2SO_3 (J.T.Baker, >99%) supporting electrolytes. Photocurrent generation of unmodified $BiVO_4$ is limited by its poor water oxidation activity and associated slow kinetics for oxygen evolution. Also, hole build-up at the interface between $BiVO_4$ and the electrolyte can lead to photocorrosion of the anode material.[16] Both issues can be overcome by addition of a sacrificial hole acceptor to the electrolyte. This way, the true potential of unmodified $BiVO_4$ as a photoanode, irrespective of its catalytic activity, can be tested. In other words, the challenge to optimise light capture and hole collection is separated from that of water oxidation catalysis. Therefore, we also collected PEC data in supporting electrolytes that contained sulfite as sacrificial hole acceptor. Select electrodes were additionally tested in 0.1 M (pH 9.2) sodium borate buffer electrolyte, prepared by adding boric acid (Sigma-Aldrich, 99%) to a solution of 15.24 g sodium tetraborate decahydrate (Sigma-Aldrich, ≥99.5%) in 400 mL water until pH 9.2 was reached. We found essentially the same PEC performance in both electrolytes, confirming that $BiVO_4$ electrodes were stable in the higher pH electrolyte during the course of the PEC measurements. Also, the stabilities of $BiVO_4$ films prepared from electrodeposition baths with added iodide did not differ from those made from plating baths without iodide during our measurements. All current density *versus* potential data were collected with rapid stirring of the liquid, to minimise mass transport effects and remove nucleated bubbles from the electrode surface; the data were not corrected for any uncompensated resistance losses. A Ni gauze (Alfa) counter electrode and a calibrated 0.1 M KOH Hg/HgO reference electrode (CH Instruments; measured at room temperature to be $E = 0.916$ V vs. RHE) were used. The calibration method has been described elsewhere.[17]

Photoanode performance was measured under simulated sunlight supplied by an Oriel Instruments model 66902 halogen light source with an ozone-free bulb; an AM1.5G filter was placed between the lamp and the photoelectrochemical cell (spectrum see below). Because of the ozone-free nature of our light source, its spectral irradiance was less intense below 500 nm, where $BiVO_4$ absorbs, than true American Society for Testing and Materials (ASTM) AM1.5G radiation. Owing to this spectral mismatch our measured photocurrents were slightly lower than true AM1.5G photocurrents would have been; this is irrelevant for the relative PEC performance comparison of this work. Electrodes were stable for at least three scans. Photocurrent values were averaged using nine or three electrodes per $BiVO_4$ preparation, in supporting electrolytes without or with sulfite, respectively; the given error bars are standard deviations. We obtained good reproducibility between electrodes and for repeated preparations.

PEC data were collected with and without illumination, and in chopped lighting conditions at 0.25 Hz, using a Wavetek model 1824A 4 MHz function generator and a Thorlabs chopper. The light source was placed at a distance from the electrode surface to achieve an incident photon flux equivalent to 1 sun illumination. Before using the solar simulator setup, the illumination intensity at the sample plane was measured by a calibrated Si photodiode (Thorlabs).

3. X-ray photoelectron spectra (XPS) of $BiVO_4$ on FTO-glass photoanodes

XPS data of $BiVO_4$ films on FTO-glass photoanodes were collected with conditions as described above. To identify which elements were present, survey scans from 0 to 1100 eV were performed. Binding energies were referenced to the C 1s peak arising from adventitious carbon, taken to have a binding energy of 284.8 eV.[13] High-resolution spectra were collected for the Bi 4d, V 2p and O 1s regions; in case of materials that were made with NaI in the electrodeposition bath, additionally high-resolution spectra were collected in the I 3d region. In the graphs, vertical dashed lines identify individual photoelectron lines; signals arising from $BiVO_4$ are labelled in black, signals from the FTO substrate underneath are labelled in grey.

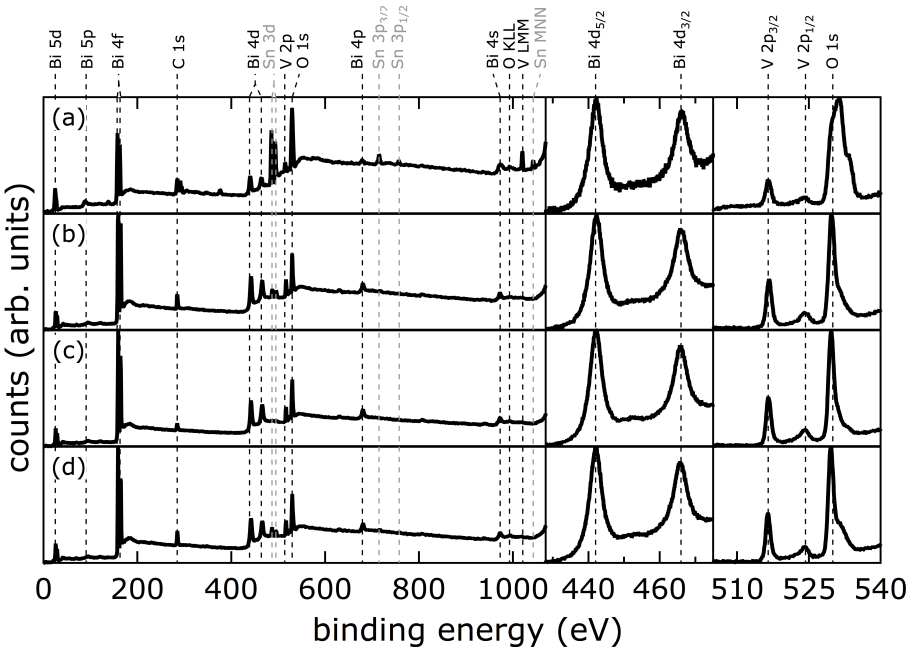

Figure S1: XPS data of spin-coated $BiVO_4$ films on FTO-glass. The films were prepared with (a) 2, (b) 4, (c) 6, and (d) 8 spin-coating cycles, without PEG in the precursor solution.

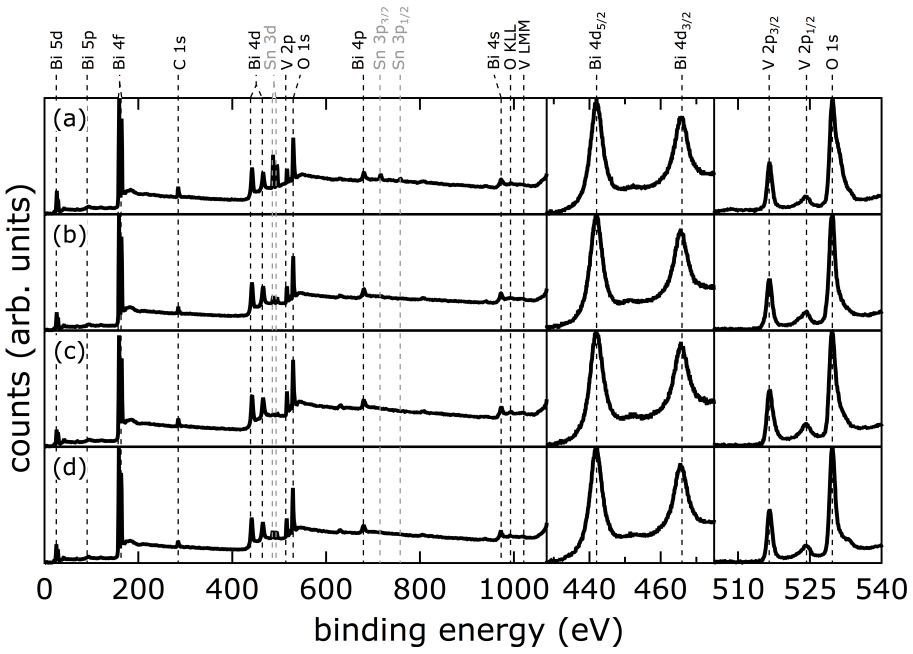

Figure S2: XPS data of spin-coated $BiVO_4$ films on FTO-glass. The films were prepared with (a) 2, (b) 4, (c) 6, and (d) 8 spin-coating cycles, with PEG in the precursor solution.

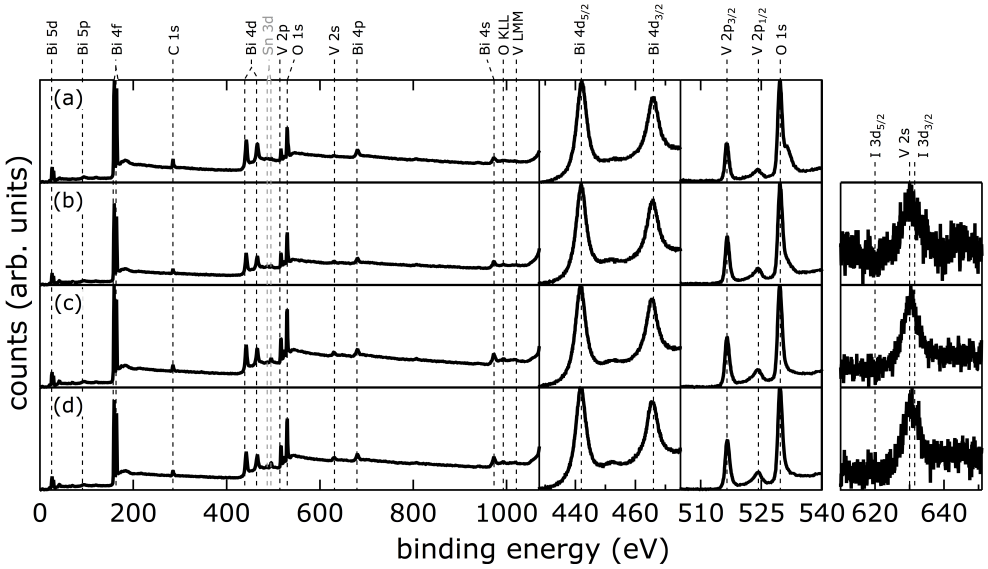

Figure S3: XPS data of electrodeposited $BiVO_4$ films on FTO-glass with different NaI concentrations in the plating bath; (a) no added NaI, $[I^-]/[Bi^{3+}]$ ratio: (b) 4, (c) 8, (d) 12.

4. X-ray diffraction (XRD) data of $BiVO_4$ on FTO-glass photoanodes

XRD data of $BiVO_4$ films on FTO-glass photoanodes were taken with conditions as described above. For comparison with spin-coated $BiVO_4$ films on FTO-glass, fixed-slit intensities of monoclinic scheelite $BiVO_4$ (PDF 00-014-0688 (ICDD, 2012), black) and rutile SnO_2 (PDF 00-041-1445 (ICDD, 2012), grey) are also displayed. XRD features of SnO_2 arise from the FTO substrates. In case of electrodeposited $BiVO_4$ films on FTO-glass with different NaI concentrations in the plating bath, additionally fixed-slit intensities of tetragonal BiOI (PDF 00-010-0445 (ICDD, 2012), blue) are shown. It becomes evident from Figure S6 that electrodeposited $BiVO_4$ films on FTO-glass with different NaI concentrations in the plating bath did not contain any contributions from crystalline BiOI.

Different types of conducting oxide substrates have been used, which makes a direct comparison of reported $BiVO_4$ PEC performance problematic. Fluorine-doped SnO_2 crystallises in tetragonal rutile structure (space group P4/nmm) with lattice parameters $a = b = 4.738$ Å and $c = 3.188$ Å (PDF 00-041-1445 (ICDD, 2012)).[18] Monoclinic scheelite $BiVO_4$, however, has the symmetry space group $I2/b$ with $a = 5.194$ Å, $b = 5.090$ Å, $c = 11.697$ Å, and $\beta = 90.387°$.[19] This lattice mismatch leads to differently shaped crystallites in the two adjacent layers. Crystallites of SnO_2 are cuboid, whereas those of our $BiVO_4$ films exhibit pillow-like morphology (see below). Depending on $BiVO_4$ crystallite size, different numbers of point contacts are formed at the interface between $BiVO_4$ and FTO. Ager studied photocurrent generation of $BiVO_4$ on tin-doped indium oxide (ITO) substrates.[8] ITO crystallites exhibit the cubic bixbyite structure of indium oxide and range in size from ~50 to several hundred nanometres, depending on preparation conditions.[20] Moreover, the electronic properties of ITO and FTO differ.[8, 21, 22].

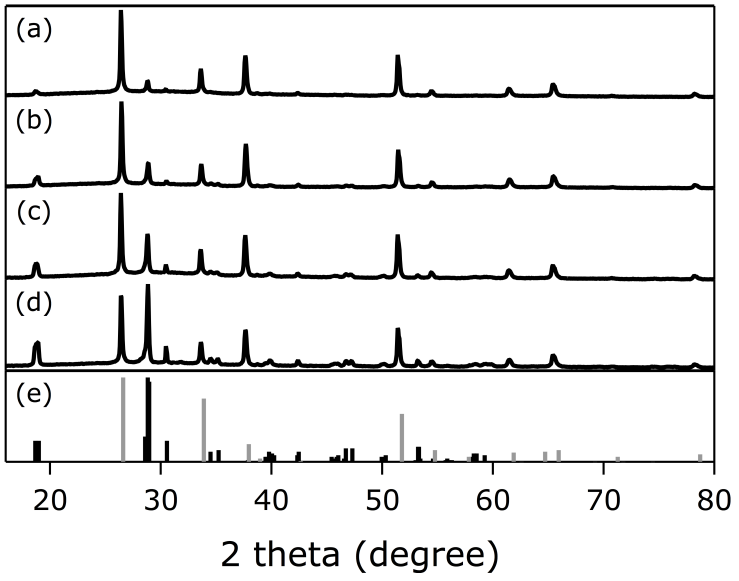

Figure S4: XRD data of spin-coated $BiVO_4$ films on FTO-glass. The films were prepared with (a) 2, (b) 4, (c) 6, and (d) 8 spin-coating cycles, without PEG in the precursor solution. (e) Fixed-slit intensities of monoclinic scheelite $BiVO_4$ (PDF 00-014-0688 (ICDD, 2012), black) and rutile SnO_2 (PDF 00-041-1445 (ICDD, 2012), grey).

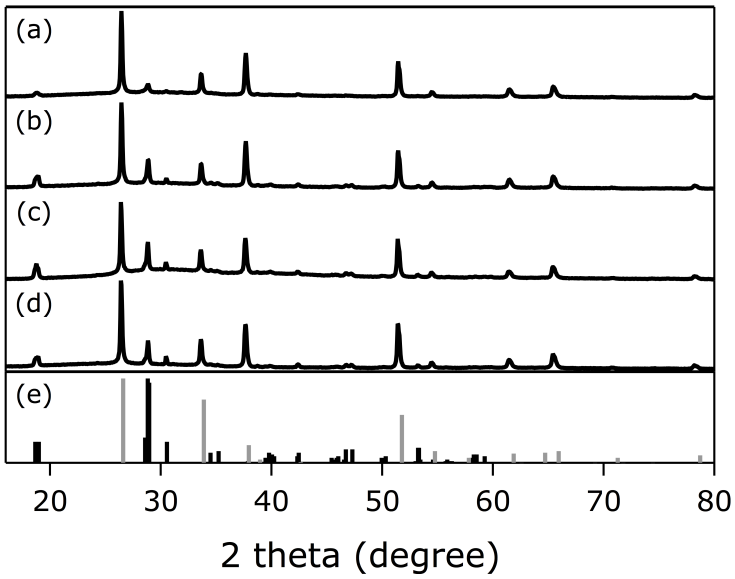

Figure S5: XRD data of spin-coated $BiVO_4$ films on FTO-glass. The films were prepared with (a) 2, (b) 4, (c) 6, and (d) 8 spin-coating cycles, with PEG in the precursor solution. (e) Fixed-slit intensities of monoclinic scheelite $BiVO_4$ (PDF 00-014-0688 (ICDD, 2012), black) and rutile SnO_2 (PDF 00-041-1445 (ICDD, 2012), grey).

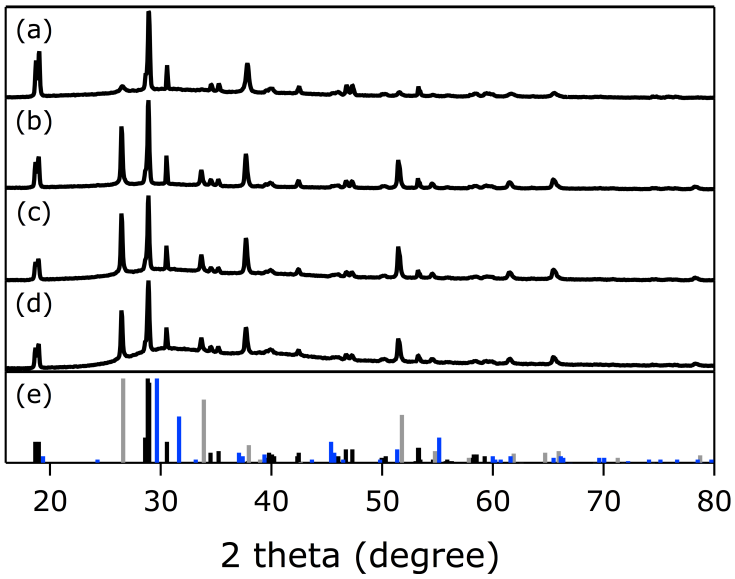

Figure S6: XRD data of electrodeposited $BiVO_4$ films on FTO-glass with different NaI concentrations in the plating bath; (a) no added NaI, $[I^-]/[Bi^{3+}]$ ratio: (b) 4, (c) 8, (d) 12. (e) Fixed-slit intensities of monoclinic scheelite $BiVO_4$ (PDF 00-014-0688 (ICDD, 2012), black), rutile SnO_2 (PDF 00-041-1445 (ICDD, 2012), grey), and tetragonal BiOI (PDF 00-010-0445(ICDD, 2012), blue).

5. Statistics of crystallite area distributions

Distributions of crystallite areas *a* were obtained from SEM images and moments were derived as described above.

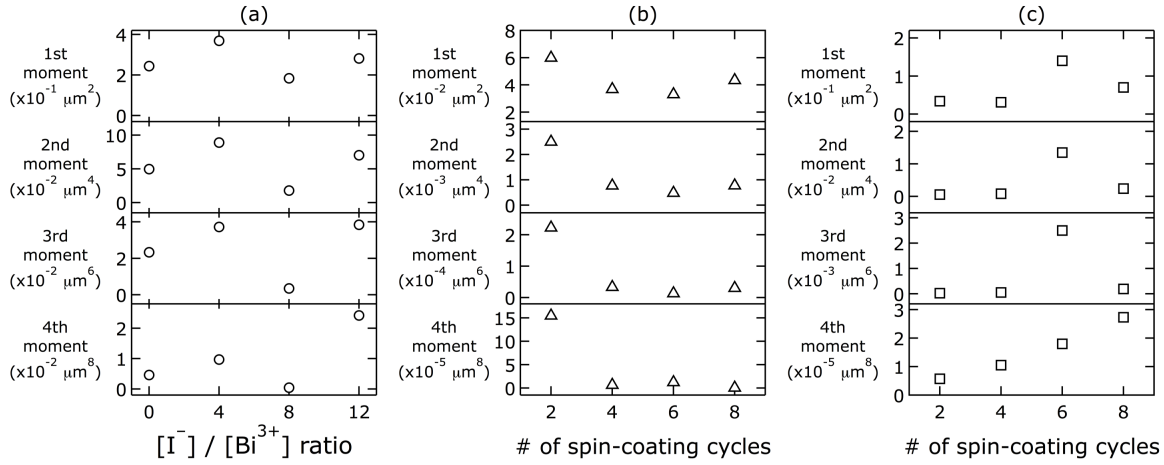

Figure S7: Statistical moments of crystallite area distributions of $BiVO_4$ films prepared by electrodeposition (a), and spin coating without (b) and with (c) PEG in the precursor solution.

6. Statistics of crystallite aspect-ratio-normalised diameter distributions

Distributions of crystallite aspect-ratio-normalised diameters *l* (defined as an ellipse's semi-minor axis divided by its semi-major axis times the square root of its area) were obtained from SEM images and moments were derived as described above.

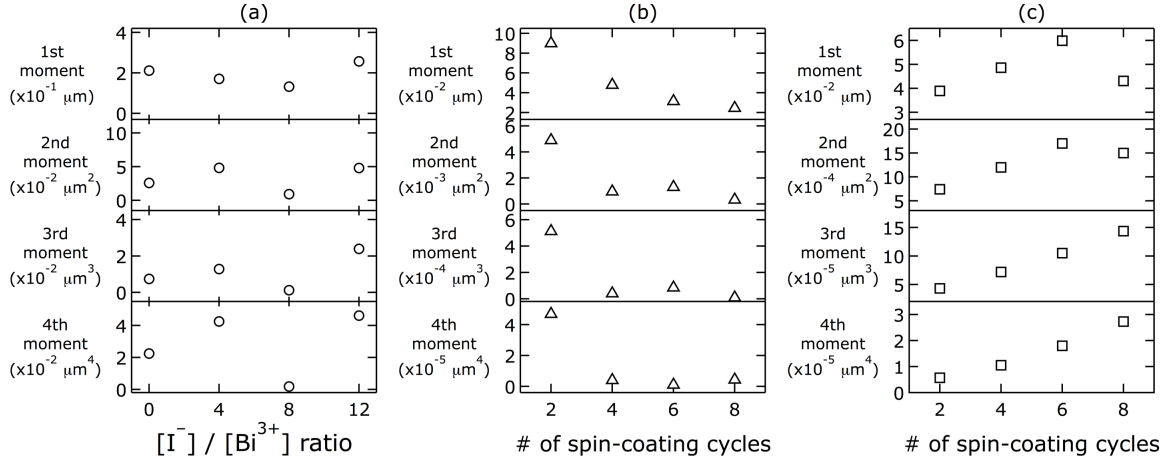

Figure S8: Statistical moments of crystallite aspect-ratio-normalised diameter distributions of $BiVO_4$ films prepared by electrodeposition (a), and spin coating without (b) and with (c) PEG in the precursor solution.

7. Optical spectra of $BiVO_4$ on FTO-glass photoanodes

Optical spectra of $BiVO_4$ films on FTO-glass were collected with conditions as described above.

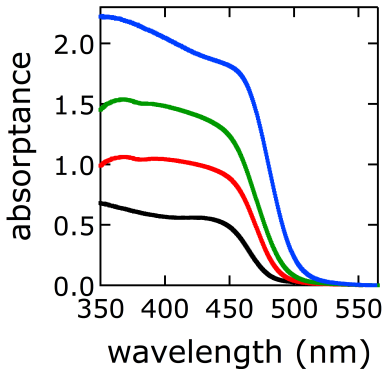

Figure S9: UV/vis absorption data of spin-coated $BiVO_4$ films on FTO-glass. The films were prepared with 2 (black), 4 (red), 6 (green), and 8 (blue) spin-coating cycles, without PEG in the precursor solution.

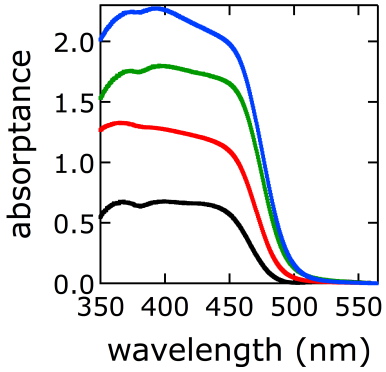

Figure S10: UV/vis absorption data of spin-coated $BiVO_4$ films on FTO-glass. The films were prepared with 2 (black), 4 (red), 6 (green), and 8 (blue) spin-coating cycles, with PEG in the precursor solution.

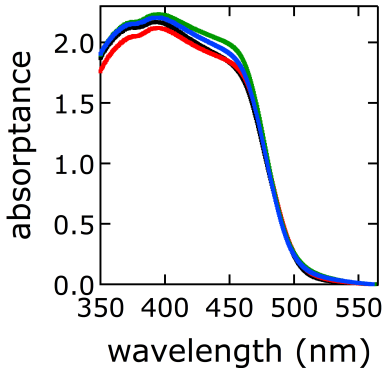

Figure S11: UV/vis absorption data of electrodeposited $BiVO_4$ films on FTO-glass with different NaI concentrations in the plating bath; black, no added NaI, $[I^-]/[Bi^{3+}]$ ratio: 4 (red), 8 (green), 12 (blue).

8. Effect of iodide on the electrodeposition baths

We prepared electrodeposited $BiVO_4$ films on FTO-glass following a procedure by Choi,[4] and, as a modification of that, with varying amounts of NaI added to the deposition bath. All other conditions were kept virtually identical and are described above. Without NaI, the deposition solution became turbid as soon as the pH was adjusted with acetate to reach anodic deposition conditions. With addition of iodide, we did not observe any precipitate throughout the plating process; solutions remained precipitate-free for hours. Photos of the plating baths with and without iodide are shown in Figure S12.

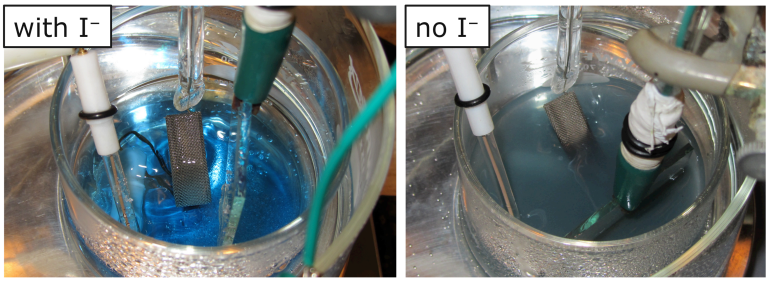

Figure S12: Photos of the electrodeposition baths with and without iodide.

9. Solubility of metal salts in the spin-coating precursor solutions

We measured the solubility of $Bi(NO_3)_3{\cdot}5H_2O$ and $VO(C_5H_7O_2)_2$ in the spin-coating precursor solvent mixtures without and with polyethylene glycol (PEG). Small amounts of $Bi(NO_3)_3{\cdot}5H_2O$ (0.3 g) and $VO(C_5H_7O_2)_2$ (0.03 g) were placed into 20 mL glass vials. Two vials were prepared with each salt, for four experiments total. The solvent mixture without PEG consisted of a 1:9 (v:v) mixture of acetic acid and 2,4-pentanedione, and the one with PEG was a 1:8:1 mixture of acetic acid, 2,4-pentanedione, and PEG. Small volumes (5-200 µL) of these mixtures were serially added to the salts. After each addition of solvent, the vials' contents were vortexed and sonicated for 5 min and brought to room temperature. After the salt dissolved completely, the final and second-to-last volumes were used to calculate the solubility and uncertainty.

Table S2. Molar solubility of metal salts in the spin-coating precursor solutions.

	$Bi(NO_3)_3{\cdot}5H_2O$	$VO(C_5H_7O_2)_2$
without PEG	(2.17 ± 0.06) M	(0.056 ± 0.005) M
with PEG	(0.87 ± 0.02) M	(0.054 ± 0.006) M

10. Dependence of photocurrent density on the interplay of morphology and chemical surface composition of electrodeposited $BiVO_4$ electrodes

Average photocurrents of electrodeposited $BiVO_4$ photoanodes were plotted in bivariate fashion as a function of quantified morphology and surface Bi/V ratio, with the aim to derive trends.

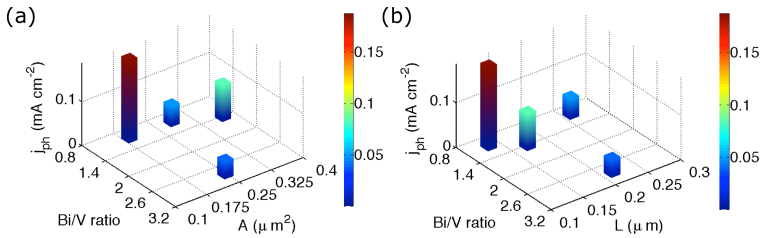

Figure S13: Dependence of photocurrent density on the morphology and chemical surface composition of electrodeposited $BiVO_4$ electrodes, without sulfite in the electrolyte. Morphology quantification: (a) mean crystallite areas *A*, (b) mean aspect-ratio-normalised diameters *L*. The bar widths are arbitrary to visualize the data.

11. Scanning electron microscopy (SEM) images of FTO on glass and $BiVO_4$ on FTO-glass

The SEM images were collected with conditions as described above.

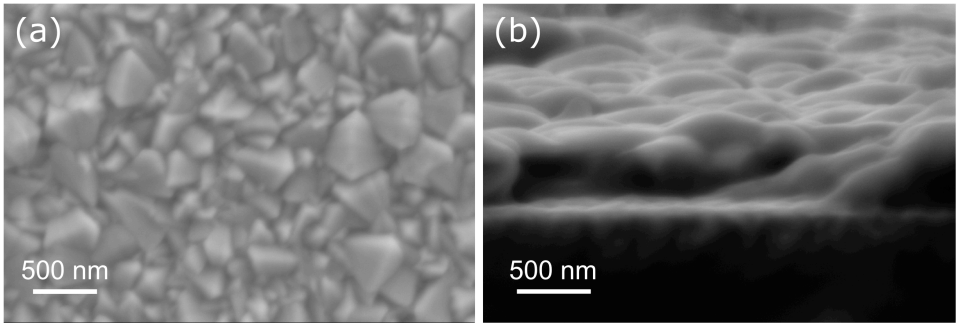

Figure S14: SEM images of (a) FTO on glass (Hartford Glass Co., TEC 15; top-down view) and (b) of electrodeposited $BiVO_4$ on FTO-glass (cross-sectional view).

12. Simulated sunlight spectrum

We used an Oriel model 66902 solar simulator with an ozone-free bulb. Figure S15 shows the emission spectrum of this simulated-sunlight source (black) and, for comparison, a reference American Society for Testing and Materials Air Mass 1.5 global spectrum (ASTM G-173, red).[23] Because of the ozone-free nature of our irradiation source, the emitted radiation was less intense in the spectral range below 500 nm than AM1.5G solar spectral irradiance. This spectral range mattered because our $BiVO_4$ photoanodes absorbed in this region (blue spectrum). As a result, our measured photocurrents were slightly lower than true AM1.5G photocurrents would have been; this is irrelevant for the relative PEC performance comparison of this work.

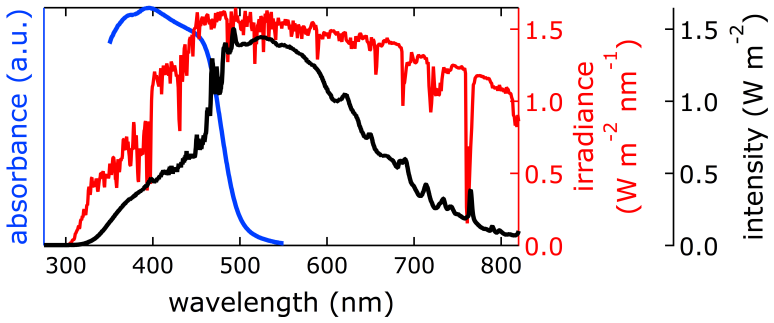

Figure S15: Simulated-sunlight spectral intensity (black) and reference solar spectral irradiance ASTM G-173 (red). Also depicted is the optical spectrum of monoclinic scheelite $BiVO_4$ (blue).

References:

1. J. Su, L. Guo, S. Yoriya and C. A. Grimes, *Cryst. Growth Des.*, 2009, **10**, 856-861.
2. K. Sayama, N. Wang, Y. Miseki, H. Kusama, N. Onozawa-Komatsuzaki and H. Sugihara, *Chem. Lett.*, 2010, **39**, 17-19.
3. S. P. Berglund, D. W. Flaherty, N. T. Hahn, A. J. Bard and C. B. Mullins, *J. Phys. Chem. C*, 2011, **115**, 3794-3802.
4. J. A. Seabold and K.-S. Choi, *J. Am. Chem. Soc.*, 2012, **134**, 2186-2192.
5. F. F. Abdi, N. Firet and R. van de Krol, *ChemCatChem*, 2013, **5**, 490-496.
6. H. W. Jeong, T. H. Jeon, J. S. Jang, W. Choi and H. Park, *J. Phys. Chem. C*, 2013, **117**, 9104-9112.
7. S. K. Choi, W. Choi and H. Park, *Phys. Chem. Chem. Phys.*, 2013, **15**, 6499-6507.
8. L. Chen, E. Alarcón-Lladó, M. Hettick, I. D. Sharp, Y. Lin, A. Javey and J. W. Ager, *J. Phys. Chem. C*, 2013, **117**, 21635-21642.
9. E. Alarcon-Llado, L. Chen, M. Hettick, N. Mashouf, Y. Lin, A. Javey and J. W. Ager, *Phys. Chem. Chem. Phys.*, 2014, **16**, 1651-1657.
10. T. W. Kim and K. S. Choi, *Science*, 2014, **343**, 990-994.
11. D. K. Zhong, S. Choi and D. R. Gamelin, *J. Am. Chem. Soc.*, 2011, **133**, 18370-18377.
12. F. C. Zumsteg, *NBS Spec. Publ. (U. S.)*, 1980, **574**, 156-159.
13. T. L. Barr and S. Seal, *J. Vac. Sci. Technol. A*, 1995, **13**, 1239-1246.
14. D. A. Shirley, *Phys. Rev. B*, 1972, **5**, 4709-4714.
15. W. S. Rasband, ImageJ; U.S. National Institutes of Health, Bethesda, MD. Available online at http://imagej.nih.gov/ij/.
16. A. Kudo, K. Ueda, H. Kato and I. Mikami, *Catal. Lett.*, 1998, **53**, 229-230.
17. J. D. Blakemore, H. B. Gray, J. R. Winkler and A. M. Müller, *ACS Catal.*, 2013, **3**, 2497-2500.
18. Joint Committee on Powder Diffraction Standards, Powder Diffraction File No. JCPDS-41-1445 (ICSD data).
19. A. W. Sleight, H.-y. Chen, A. Ferretti and D. E. Cox, *Mater. Res. Bull.*, 1979, **14**, 1571-1581.
20. M. Bender, J. Trube and J. Stollenwerk, *Thin Solid Films*, 1999, **354**, 100-105.
21. K. Reimann and M. Steube, *Solid State Commun.*, 1998, **105**, 649-652.
22. P. D. C. King, T. D. Veal, D. J. Payne, A. Bourlange, R. G. Egdell and C. F. McConville, *Phys. Rev. Lett.*, 2008, **101**, 116808.
23. Spectral data from http://rredc.nrel.gov/solar/spectra/am1.5/ASTMG173/ASTMG173.html.